MEMS-Based Acetone Vapor Sensor for Non-Invasive Screening of Diabetes

Almur A. S. Rabih, *Member, IEEE*, J. O. Dennis, *Senior Member, IEEE*, A. Y. Ahmed, *Member, IEEE*, M. H. Md Khir, *Member, IEEE*, Mawahib G. A. Ahmed, *Member, IEEE*, Alamin Idris, and Muhammad Umer Mian, *Member, IEEE*

***Abstract*— Acetone vapor sensing is important for environmental monitoring and non-invasive screening of diabetes mellitus (DM). Inhaling higher than 176 parts per million (ppm) acetone concentrations affects the respiratory system, while acetone in exhaled breath correlates with blood glucose and exhaling more than 1.8 ppm indicates the person is in danger of DM. DM is currently diagnosed invasively by measuring glucose level in blood, which is painful, and therefore inconvenient. This paper reports MEMS sensor device functionalized with blend of Chitosan/Polyethylene glycol polymers for acetone vapor sensing for possible non-invasive screening of diabetes. The sensor was experimentally tested using synthetic acetone vapor, and found to give linear response for 0.05–5 ppm acetone in air, with a sensitivity of 21 mV/ppm, good repeatability, response, and reversibility. Cross-sensitivity for 2-propanol and methanol was examined, where the responses of the sensor to 1 ppm concentration in air of these two analytes were found to be 24% and 33%, respectively, less compared to its response to the same concentration of acetone.**

***Index Terms*— MEMS sensor device, Chitosan/Polyethylene glycol, micro-device, Acetone vapor, diabetes screening.**

I. Introduction

DIABETES or diabetes mellitus (DM) is the main cause of mortality and morbidity worldwide in the modern era, and it is expected to affect about 552 million by the year 2030 [1]. It is caused by deficiency of insulin production or by improper use of insulin by body tissues. Deficiency of insulin occurs due to destruction of the pancreatic β cells responsible for insulin production by the body immune system. Lack of insulin causes glucose concentration in blood to become high and it can lead to serious health problems such as blindness, kidney failure, heart diseases, premature death, limb amputation and gangrene [2]. When blood glucose concentration exceeds 100 milligram per deciliter (mg/dL) the person is diagnosed as diabetic on a chronic basis [3]. Genetics, environmental and habitual factors such as lack of exercise and obesity are believed to play a major role in developing DM. DM has three main types. Type 1 diabetes, also called juvenile diabetes is insulin dependent and it affects $5 - 10$ % of the diabetic people. It occurs due to inability of the pancreas to excrete insulin, which requires the patients to take insulin for the rest of their lives. Diabetic ketoacidosis is the late stage of this type, and it is characterized by accumulation of acetoacetate (AcAc), beta-hydroxybutyrate (β-OHB) and acetone in the body fluids. Concentration of AcAc and β-OHB in the body fluids is reflected by the pH and electrolyte concentrations in arterial blood, while spontaneous and probably nonenzymatic decarboxylation of AcAc leads to elevation of acetone concentration in the blood [4]. Type 2 diabetes is called insulin independent diabetes, and it affects $90 - 95$% of the diabetic people. It occurs due to excretion of insufficient insulin by pancreas or due to the cell resistance to the insulin to carry glucose. Type 3 diabetes is called gestational diabetes which infects pregnant women at their last stage of the pregnancy (trimester).

A. History of Diagnosis of Diabetes

Diabetes was first diagnosed through examining urine samples by looking at its appearance, colour and sediment to observe glucose presence. Urine test was found to suffer many limitations, such as test result is affected by fluid intake and urine concentration, where urine glucose only reflects current glycaemic status, and positive results only occur when a certain glucose threshold in urine is reached, and negative results does not differentiate between hyperglycemia, euglycemia and hypoglycemia. Hence the focus was shifted from the urine test and have been concentrated more on the blood testing since 19^{th} century till present date [5].

Blood glucose test was first introduced in 1965 by Ames research team using a paper reagent strip based on glucose/peroxidase reaction [5]. Currently, diabetes is diagnosed invasively by withdrawal of venous blood and then the glucose concentration is analyzed using glucose analyzers, or alternatively by using the handheld glucose meters. Blood glucose measurement takes one of three forms; fasting plasma glucose blood test (FPG), oral glucose tolerance test (OGTT), or Hemoglobin A1C (HbA_{1C}) test [6]. FPG is preferred for diabetes diagnosis because it is convenient and low cost. However, the test requires patients to fast for long time

Manuscript received July 19, 2018; accepted August 31, 2018. Date of publication October 2, 2018; date of current version November 13, 2018. This research is supported by Universiti Teknologi PETRONAS (UTP), through the University Research Internal Fund (URIF) under project cost-center 0153AA-G29. The associate editor coordinating the review of this paper and approving it for publication was Prof. Mehdi Javanmard. *(Corresponding author: Almur A. S. Rabih.)*

A. A. S. Rabih and M. G. A. Ahmed are with the Department of Electronic Engineering, Faculty of Engineering and Technology, University of Gezira, Wad Madani, Sudan (e-mail: almurutp@gmail.com).

J. O. Dennis is with the Department of Fundamental and Applied Sciences, Faculty of Science and Information Technology, Universiti Teknologi PETRONAS, Seri Iskandar 32610, Malaysia.

A. Y. Ahmed, M. H. Md Khir, and M. U. Mian are with the Department of Electrical and Electronic Engineering, Faculty of Engineering, Universiti Teknologi PETRONAS, Seri Iskandar 32610, Malaysia.

A. Idris is with the Department of Chemical Engineering, Faculty of Engineering, Universiti Teknologi PETRONAS, Seri Iskandar 32610, Malaysia.

Digital Object Identifier 10.1109/JSEN.2018.2870942

TABLE I
WHO CRITERIA FOR DIAGNOSIS OF DIABETES [10]–[12]

Test	Unit	Condition			
		Normal	IFG	IGT	DM
FPG	mmol/l	< 6.1	≥ 6.1&<7.0	≤ 7.0	≥ 7.0
OGTT	mmol/l	< 7.8	< 7.8	≥7.8	≥ 11.1
HbA_{1C}	mmol/mol	< 42	42 – 46	42 – 46	≥ 48
	DCCT%	< 6.0	6.0 – 6.4	6.0 – 6.4	≥ 6.5

(8 hours) prior to drawing blood sample for glucose test examinations [7]. Blood glucose below 100 mg/dL indicates the subject is normal, 100-125 mg/dL indicates that the subject has impaired fasting glucose (IFG) which means the subject is in pre-diabetes stage, and 126 mg/dL is considered as a threshold for the diabetes mellitus (DM). It is often the first test done to diagnose pre-diabetes and diabetes. In OGTT, after the subjects fast for 8 hours they are asked to drink a liquid contains 75 g glucose, take 2 hours rest time and then the blood is drawn for glucose test. It is used to distinguish between metabolically healthy individuals and those who have impaired glucose tolerance (IGT) or diabetes. This method is not recommended for routine diagnosis. Glucose level below 140 mg/dL is considered normal, between 140mg/dL and 199 mg/dL describes the pre-diabetes IGT stage [3] and the threshold of the diabetes glucose is 199 mg/dL. HbA_{1C} is the most accepted and recommended test by World Health Organization (WHO) and American Diabetes Association (ADA) as an alternative way to FPG and OGTT for diabetes detection. It is more stable, doesn't need the patient to fast, and it also needs small amount of blood for the diagnosis [8]. HbA_{1C} measures glucose percent in the blood over the period of past three months; hence the result is not affected by biological variations which associate with fasting. Values greater than 6.4% indicate diabetes, $5.5 - 6.4\%$ is pre-diabetic state and less than 5.5% is normal [9].

TABLE I summarizes the criteria of the World Health Organization (WHO) for the diagnosis of diabetes.

Blood glucose testing rely either on bench top glucose analyzers or handheld glucose meters. The handheld meters use lancet to prick the fingertip and the blood is wiped with a strip containing substances that reactive to glucose. These methods depends on electrochemical reactions [13]. Disadvantages of invasive methods are patients discomfort [14], risk of infection and inaccuracy due to multiple test times per day [15] and over long time use the finger tissue is at risk of damage [1]. In addition glucose meters experience lack of measurement accuracy, temperature effect causes false results and high cost of consumables [16]. Due to the issues discussed above many non-invasive methods for blood glucose testing were recommended. Those non-invasive techniques includes bio impedance spectroscopy, electromagnetic sensing, fluorescence technology, mid-infrared spectroscopy, near infrared spectroscopy, optical coherence tomography, reverse iontophoresis, optical polarimetry, Raman spectroscopy and ultrasound technology [1]. Some of the main limitations of the non-invasive methods are: bioimpedance spectroscopy and electromagnetic sensing are affected by body temperature and body water contents, fluorescence technology suffers from strong scattering phenomena [1], and infrared technology lacks of accuracy and stability [17]. In addition, Raman spectroscopy lacks precision and specificity that is found in the invasive glucose meters [14]. For those reasons the invasive blood glucose test is still practiced by clinician for the diabetes screening and monitoring. However, efforts are still being put in place to develop reliable non-invasive methods for diabetes screening. An example is measuring acetone vapor in exhaled breath which was found to linearly correlate to the glucose concentration in the blood.

B. Acetone Vapor Sensing in Exhaled Breath for Diabetes Screening

Exhaled breath (EB) is a bulk mixture of inorganic compounds (nitrogen, oxygen, carbon dioxide), inert gases and more than 1000 volatile organic compounds (VOCs) ranged from part per million (ppm) to part per trillion (ppt) in concentrations. Exhaled breath analysis (EBA) is non-invasive, real time detection, and least harmful compared to its rivals blood or urine tests [18]. Its use is increasing in the recent years for state of disease monitoring or exposure to drugs or environmental pollutants [19], by analyzing and studying the potential biomarkers existed in EB. For instance, exhaled nitric oxide (NO) and hydrogen peroxide were identified as biomarkers for oxidative stress that associated with inflammatory lung diseases [20]–[22]. Exhaled ammonia was used as a useful biomarker for kidney diseases [23] and exhaled acetone was found to relate and reflect ketone bodies in blood plasma, blood acetone levels, and β-hydroxybutyrate in venous blood. As a result, breath acetone linearly correlates to glucose in blood and can offer a solution to the invasive blood glucose measurement for better treatment and control of diabetes [24], [25]. Acetone concentration in ambient air is 7.34 parts per billion (ppb), in normal subjects is ranged $0.22 - 0.8$ ppm with mean of 0.51 ppm, and in diabetic patients it is $1.76 - 3.73$ ppm with mean of 2.35 ppm [26].

Several techniques have been used to detect acetone in exhaled human breath for diabetic screening. The most common used methods include gas chromatography (GC) with flame ionization detection (FID), mass spectroscopy (MS), ion mobility spectroscopy (IMS), or combinations like GC-MS, proton transfer reaction-mass spectroscopy (PTR-MS) and selected ion flow tube mass spectroscopy (SIFT-MS) [18], [27]. Deng *et al.* [26] used GC-MS and solid-phase micro extraction (SPME) to detect breath acetone. Acetone was extracted by polydimethylsiloxane-divinylbenzene (PDMS-DVB) fiber and reacted with O-2, 3, 4, 5, 6-(pentafluorobenzyl) hydroxylamine hydrochloride (PFBHA) to form acetone oxime which is easy to analyze by GC-MS. They found the acetone concentration for diabetic subjects to be higher than 1.71 ppm and for the normal subject to be lower than 0.76 ppm. Galassetti *et al.* [28] used GC-MS technique to detect acetone concentration in exhaled breath for diabetes screening. Patients were asked to breath into specially designed electropolished stainless steel canisters and the samples stored at room temperature for analysis within $2 - 3$ weeks. OGTT test was conducted for 10 healthy subjects by ingesting 75 g of glucose and measurements were done

within 120 minutes. The acetone concentration in the breath was found to relate to blood glucose by 0.41 − 0.95 correlation factor. SIFT-MS was used to monitor breath of 8 patients with Type 1 diabetes by another researcher [2]. Exhaled acetone was found to decline as the glucose intake was decreased. Non fasting average of acetone breath in healthy individuals has been found to be in a range of 0.148 − 2.744 ppm with an average of 0.477 ppm [2]. Another study was conducted by Musa-Veloso *et al.* [29] using GC equipped with FID to observe the relation of breath acetone, urinary acetoacetate with ketones acetoacetates and β-hydroxybutyrate, and also to see the effect of consumption of ketogenic diets used for treatment of intractable seizures on acetone concentration. Breath was collected using Easy sampler bags made from polyethylene. Plasma acetoacetate has been found to correlate to exhaled breath acetone by 0.70 and exhaled breath acetone increased from 33 ± 13nmol/l to 116 ± 19nmol/l after 12 hrs of consuming the diets. Although above methods are sensitive, they are still costly, heavy and table top equipments, and require longer time for sample preparation [18]. Methods based on laser spectroscopic techniques, electrochemical sensors, surface acoustic wave, quartz microbalance and semiconductor sensors were also studied extensively to find alternatives to GC-MS techniques [30].

Resonant mass sensors such as MEMS resonators, quartz crystal microbalance (QCM), bulk acoustic (BAR) and surface acoustic wave (SAW) devices have gained a significant interest in the field of mass sensing applications due to their intrinsic high sensitivity and wide deployment in numerous apparatus and instruments [31]. The working principle of these devices is based on frequency shift detection as a result of mass loading. D'Amico *et al.* [32] reported QCM resonator coated with CNTs layer films for ethanol, methanol, acetone, m-xylene, toluene and ethyl acetate gases in a broad range of 10 − 800 ppm. The measurement was conducted at room temperature and the concentration range of the acetone gas was 240 − 720 ppm. Kosuru *et al.* [33] used QCM coated with poly-4-vinylpyridine (PVP) and metal organic framework HKUST-1 as a sensitive layer for humidity sensing. Ying *et al.* [34] used QCM resonator coated with poly (epichlorohydrin) (PECH) for acetone vapor sensing in the range of 0.2 to 1.2 mg/m3 (0.08 ppm − 0.5 ppm).

II. Modeling and Fea Simulation of the Device

In this section, design, mathematical modeling and simulation of the device are presented. The device is designed following polysilicon multi-user micro electro-mechanical system processes (PolyMUMPs) technology provided by MEMSCAP. The typical thicknesses of all the PolyMUMPs layers are shown in Table II.

The schematic of the device is shown in Fig.1. It consists of a square moving plate supported by four flexible beams, and suspended on top of a fixed plate with an initial gap.

The top plate is made of only Poly 2 and Gold layers ($\sim 2\mu$m), while the bottom fixed plate is made of Poly 0 layer. The initial gap between the top moving and bottom fixed plates is $\sim 4.75\mu$m created due to absence of First Oxide,

TABLE II
Typical Thickness of the PolyMUMPs Layers

Layer	Thickness (μm)
Nitride	0.6
Poly 0	0.5
PSG	2.0
Poly1	2.0
Second Oxide	0.75
Poly 2	1.5
Metal (Gold)	0.5

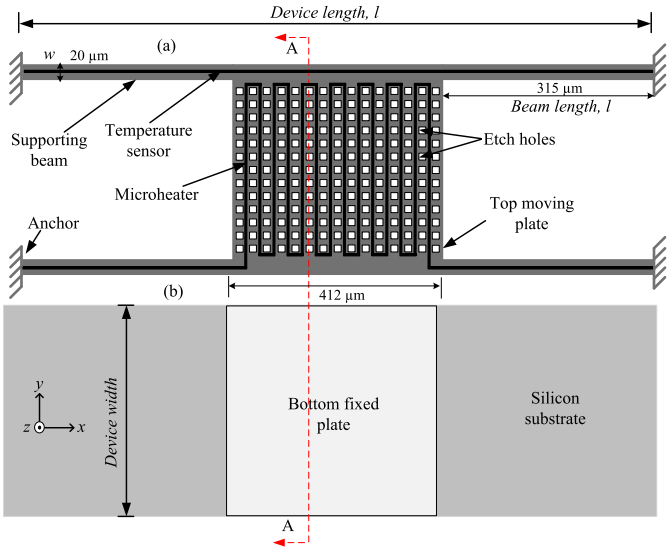

Fig. 1. Schematic of the device: (a) moving plate and (b) the bottom fixed plate.

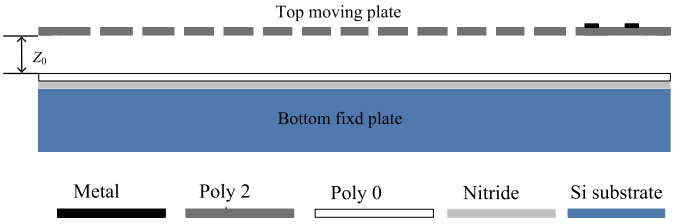

Fig. 2. Cross section A–A of the device.

Poly 1 and Second Oxide layers in this proposed design. The actuation mechanism of the device was achieved electrothermally by incorporating a microheater on top of the moving plate (Fig. 1). The cross section views A—A of the device is show in Fig. 2. The dimensions of the device, heater and temperature sensor are show in Table III.

A. Modeling of the Device

Since the upper moving plate is supported by four beams, and the aspect ratio of the thickness to width of the beams is 0.075, the upper plate moves vertically in the direction of z axes as shown in Fig. 1.

1) Resonance Frequency of the Device: Due to the vertical movement of the moving plate, the plate experiences squeeze film damping occurs between this plate and the bottom

TABLE III
DIMENSIONS OF THE DEVICE

Parameter	Dimension (μm)
Device length	1042
Device width	412
Plate area	412 × 412
Stator to moving plates gap	4.75
Length of beams	315
Width of beams	20
Thickness of beams	1.5
Temperature sensor length	1042
Temperature sensor width	4
Temperature sensor thickness	0.5
Micro-heater length	8662
Micro-heater width	4
Micro-heater thickness	0.5

fixed plate. By considering this damping, (1) is used to find the resonance frequency of the device [35].

$$f = \frac{1}{2\pi}\sqrt{\frac{k}{m} - \frac{b^2}{4m^2}} \tag{1}$$

where k is the spring constant of the four beams, m is the total mass of the coated device and b is the squeeze film damping. The spring constant k of the device supported by four beams, and in the vertical movement is found by (2) [36].

$$k = 4\frac{E_{avg} w_{avg} t^3}{l^3} \tag{2}$$

where E is the Young's modulus of Poly 2, w, t, and l are the width, thickness and length of the beams.

The total mass m of the device is a summation of the effective mass $m1$ of the four supporting beams, the static mass $m2$ of the moving plate and the mass $m3$ of a sensing layer deposited on top of the moving plate. To find the effective mass of the four fixed-guided beams, (3) is used [37], [38], and for the static mass of the moving plate and the mass of the sensing layer, (4) and (5) are used, respectively.

$$m1 = 4 \times \frac{13}{35}\rho l w t \tag{3}$$

$$m2 = \rho A t \tag{4}$$

$$m3 = \rho_3 A_3 t_3 \tag{5}$$

where ρ is the density of Poly 2, A is the area of the moving plate, ρ_3 is the mass density of the sensing layer, A_3 is the deposited area of the moving plate and t_3 is the thickness of the deposition.

The squeeze film damping of the uniformly perforated thin film plate is found using (6) [39].

$$b = \frac{3\eta A^2}{2\pi z_0^3 N} k(\beta) \tag{6}$$

where η is the dynamic viscosity of the fluid, and for air is equal to 1.8×10^{-5}Pa.s at 1 atmospheric pressure and 20°C [40], A is the area of the moving plate, z_0 is the initial gap between the moving plate and the bottom fixed plate. N is the number of perforations holes and $k(\beta)$ is a factor that depends on the radius of perforations, found by (7).

$$k(\beta) = 4\beta^2 - \beta^4 - 4\ln\beta - 3 \tag{7}$$

where $\beta = r_o/r_c$, r_o is the radius of each perforation hole, and r_c is the radius of circular cell surrounding each hole.

2) Mass Sensitivity and Quality Factor of the Device: The mass sensitivity S_m determines the ability of the device to detect small mass changes, and it is found by taking the derivative of (1), as expressed in (8).

$$S_m = \frac{\partial f}{\partial m} = \frac{(b^2 - 2km)}{4\pi m^2\sqrt{4km - b^2}} \tag{8}$$

The quality factor Q is defined as the ratio of the resonance frequency f to the bandwidth BW as expressed by (9) [41].

$$Q = \frac{f}{BW} = \frac{f}{f_2 - f_1} \tag{9}$$

where the bandwidth is determined by the frequencies f_1 and f_2 at which the voltage gain is 0.707 of the maximum. Under the influence of damping Q can be determined by (10).

$$Q = \frac{\sqrt{mk}}{b} \tag{10}$$

3) Vapor Concentration Sensitivity and Detection Limit of the Device: The vapor concentration sensitivity S_g determines the ability of the device to detect small changes of acetone concentrations in the ambient environment. It is defined as the change in the resonance frequency due to the change of the acetone vapor concentration as shown by (11).

$$S_g = \frac{\partial f}{\partial C_g} = \frac{\partial f}{\partial m} \times \frac{\partial m}{\partial C_g} \tag{11}$$

Equation (11) gives the vapor concentration sensitivity in Hz/g/m^3. To convert it to the widely accepted unit of Hz/ppm (12) is used [42].

$$S_g = \frac{(b^2 - 2km)}{4\pi m^2\sqrt{4km - b^2}} \times K V_P \frac{WP}{RT \times 10^6} \tag{12}$$

where W is the molecular weight of the acetone vapor in g/mol, P is the partial pressure (in Pascal) of the acetone vapor at the given temperature T(in Kelvin), and R is the ideal gas constant having the value of 8.3145 J.mol^{-1}K^{-1}. K is the partition coefficient of the analyte (acetone vapor)-polymer (coating layer) interface. K ranges from $100 - 10000$ for specific analyte-polymer interactions [42].

The Limit of detection $C_{g\,\min}$ determines the minimum amount of the acetone vapor that the device is capable to detect, and it depends on the minimum frequency shift detected (resolution) by the frequency measurement instrument. Equation (13) is used to calculate the minimum detectable concentration of acetone vapor (in ppm).

$$C_{g\,\min} = \frac{\Delta f\left(4\pi m^2\sqrt{4km - b^2}\right)}{K V_p\left(b^2 - 2km\right)} \times \frac{RT \times 10^6}{WP} \tag{13}$$

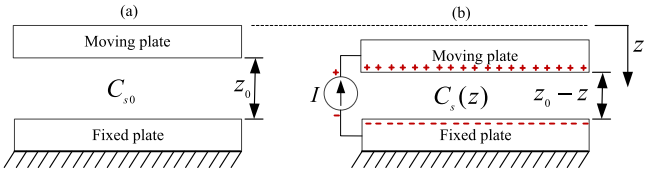

Fig. 3. Moving and fixed plates of the device showing (a) initial condition and (b) after displacing the moving plate due to actuation.

The actuation of the device was achieved using electrothermal means by having the microheater shown in Fig. 1. The advantages of electrothermal actuation are large plate displacement [43], ease of fabrication and relatively low applied voltage [44]. The actuation occurs due to thermal force caused by temperature difference generated by applying a voltage across the terminals of the microheater. This temperature difference ΔT is found by knowing the thermal resistance R_{th} of the device and the heating power P as shown in (14).

$$\Delta T = R_{th} P \tag{14}$$

The heating power depends on the applied current, dimensions of the microheater and also on the resistivity of the material made the microheater as shown by (15).

$$P = I^2 R = I^2 \frac{\rho_h l_h}{w_h t_h} \tag{15}$$

where I is a current passed through the microheater, R is the electrical resistance of the microheater, ρ_h, l_h, w_h and t_h are the resistivity, length, width and thickness, respectively of the microheater.

The output signal of the device is detected by measuring the change in the capacitance between the top moving and the bottom fixed plates. Capacitive sensing is the most common sensing methods in MEMS applications due to its compatibility with all the fabrication processes and robustness [45]. The main advantages of the capacitive sensing are simplicity in design, high sensitivity, low drift and low temperature effect. Due to actuation, the top moving plate is displaced out of plane by z (Fig. 3) and hence the initial gap changes which leads to change in the static capacitance.

As shown above in Fig. 3, initially when there is no actuation (Fig 3 (a)), the gap between the moving and fixed plates is z_0 which results in the static capacitance (C_{s0}). When the moving plate is displaced by z (Fig 3 (b)), the change in capacitance $C_s(z)$ is found by (16).

$$C_s(z) = \frac{\varepsilon_0 A_s}{z_0 - z} = C_{s0} \frac{z_0}{z_0 - z} \tag{16}$$

Some of the material properties of the PolyMUMPs layers used for this device are shown in TABLE IV.

B. FEA Simulation of the Device

To simulate the device, the designer tool of 2008 CoventorWare software was used. CoventorWare is an integrated suite of software suitable for use to simulate MEMS and microfluidics devices. It is a virtual fabrication environment that used to mimic the real design world to reduce the design faults, manufacturing time and also to reduce the cost of the fabrication by anticipating and rectifying any design risks involved by using finite element analysis.

TABLE IV
MECHANICAL AND THERMAL PROPERTIES OF POLYMUMPS LAYERS [44]

Materials	Poly 0	Poly 2	Gold	Unit
Young's modulus	158	158	57	GPa
Density	2230	2300	19300	kg/m^3
Electrical conductivity	6.667	3.33	3305	10^4S/m

III. FABRICATION, PREPARATION OF SENSING LAYER AND CHARACTERIZATION OF THE DEVICE

The device was fabricated by MEMSCAP Company, USA using PolyMUMPs fabrication technology, which is a three-layer polysilicon surface micromachining process. On the other hand, the characterization was carried in Universiti Teknologi PETRONAS, Malaysia using probestation with other electronic equipments.

A. Fabrication Steps

The fabrication normally starts by depositing 0.6 μm film of silicon nitride on a heavily-doped silicon substrate. The nitride serves as a dielectric isolation layer. Then the first polysilicon layer (Poly 0) of 0.5 μm is deposited via Low Pressure Chemical Vapor Deposition (LPCVD) and patterned using Reactive Ion Etching (RIE). After that, 2 μm of conformal Phospho-Silicate Glass (PSG) is deposited as the first sacrificial layer. Portions of the PSG are then etched so that the subsequently deposited polysilicon (Poly 1) can be anchored to the nitride or Poly 0 layers. A 1.5 μm thick conformal polysilicon (Poly 2) is subsequently deposited and patterned. Gold is the final layer deposited for probing, electrical routing, micro-heater element and temperature sensor. At the end of depositions of all layers, the sacrificial PSG layer is etched away using Hydrofluoric acid (HF) solution to release the moving plate (Poly 2) and Gold layers, leaving freestanding beams anchored to the substrate through Poly 2, Poly 1, Poly 0 and nitride layers. Fig. 4 shows FESEM image of the fabricated device.

B. Preparation and Deposition of the Sensing Layer and Characterization of the Sensor Device

Using MEMS devices for mass sensing applications requires chemical or physical modification of the device surface by a material sensitive to the targeted molecule of detection [46]. For this study, the device was deposited with a blend of chitosan (CH) and polyethylene glycol (PEG) polymers as sensing layer for acetone vapor sensing. Medium molecular weight Chitosan and Polyethylene glycol of molecular weight ranged from 6550 to 536000 Dalton and Acetic acid glacial were purchased from Sigma Aldrich, Malaysia.

Chitosan is an attractive abundant natural polymer due to its low cost, non-toxicity, biodegradability, biocompatibility,

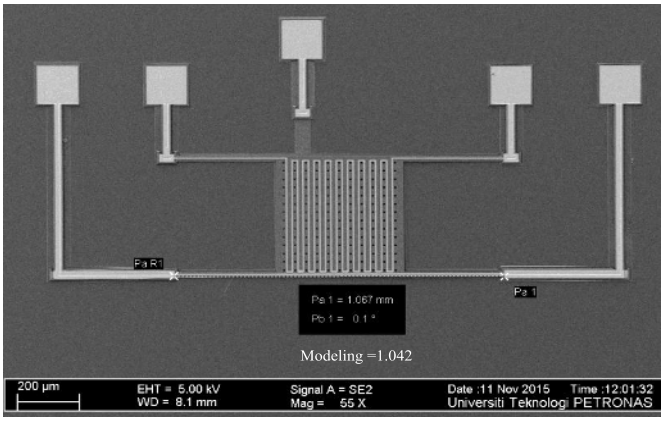

Fig. 4. FESEM of the fabricated device.

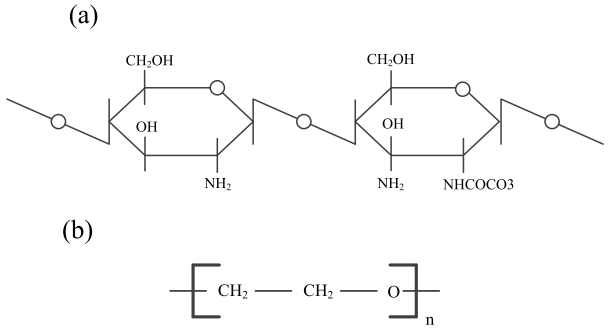

Fig. 5. Chemical structure (a) of chitosan and (b) of PEG/PEO.

anti-bacterial and hydrophilicity [47]. It is the second most bountiful polysaccharide after cellulose, made from naturally occurring resources like exoskeleton of insects, arthropods such as crustacean shells, and shellfish like shrimps, prawns, crabs and beaks of cephalopods, in addition to cell walls of fungi [48].

Polyethylene glycol is a group of water-soluble polymers that have wide range of molecular weights (200-7000000 g/mol) with valuable properties such as protein resistance, immunogenicity and low toxicity [49]. Depending on its molecular weight, it is called Polyethylene oxide (PEO) when the molecular weight is >200,000 g/mol, and Polyethylene glycol (PEG) for the lower molecular weights [50]. Figure 5 shows the chemical structure of chitosan [51], and the chemical structure of PEG/PEO.

The sensing layer is made by firstly dissolving 500 mg of the chitosan powder in 9 ml of 2% acetic acid glacial. Then, 10 mg of PEG was dissolved in 1ml deionized water. Then the two solutions of the CH and the PEG were mixed to make the blend. The mixture was put on a magnetic stirrer for 24 hours to obtain a homogeneous solution of the CH and PEG. Then after the 24 hours the mixture was put inside a sonicator for 10 seconds to remove the trapped micro bubbles created during the stirring process. The prepared material was found to be transparent, yellowish color and has jelly shape.

Prior to depositing the device, characterization is performed to investigate the functionality of the device. It was performed inside a clean booth environment of a controlled humidity and temperature. The characterization started by connectivity measurement to check the electrical connections such as checking the resistance of microheater and temperature sensor and the electrical connections of capacitor plates. Then it was followed by wire bonding of the device using West bond wirebonder to package the device for better connections to the test jig.

The sensing layer was deposited on top of the moving plate of the device using drop coating technique under a microscope. Fig.6 shows FESEM image of the deposited device, where the diameter of the deposited layer is $\sim 300 - 390\ \mu$m.

The deposited sensing layer was characterized using x-ray spectroscopy to study the composition of the sensing layer as shown in Figure 7. The major constituent of the sensing layer is carbon (C) is the weight and atomic percentages of 47.0% and 57.11 %, respectively compared to the other constituents. Carbon is the backbone of the polymer materials used to prepare the sensing layer.

The output signal of the device was detected by using MS3110 capacitive readout circuit to convert the change of the capacitance to a change in a voltage. The output voltage of the readout circuit was then amplified and displayed by network analyzer model SR770 following the measurement setup shown in Fig. 8.

The MS3110 is ultra-low noise CMOS IC used to support various MEMS sensors that require high resolution capacitive readout interface circuit. It requires only a single +5 V DC to operate it, which is given through USB cable connected to a computer, and no additional components are required. Fig. 9 shows the schematic circuit of this IC. There are two input capacitors (C_{s1} and C_{s2}), connected in parallel with sensor capacitance (C_1) and reference capacitance (C_2), respectively. The output voltage V_o of this readout circuit is given by (17).

$$V_o = \frac{1.14GV_{REF}(C_{T2} - C_{T1})}{C_F} + V_{REF} \tag{17}$$

where G is the internal gain of the circuit equals 2 or 4; in our case it was set to be 2, C_F is adjustable feedback capacitor; set to be 5.13 pF, V_{REF} is reference voltage set to be 2.25V. C_{T2} is the parallel summation of the reference capacitance C_2; 1 pF and the internal input capacitance C_{s2}; 0.798 pF, while C_{T1} is the parallel summation of the sensor capacitance C_1; 0.317 pF and the internal capacitance C_{s1}; 2.052 pF.

C. Experimental Testing of the Sensor Device

Experiments were conducted to test the performance of the deposited sensor device for small concentrations of acetone vapor. The tested concentrations are in the range of acetone concentrations of the diabetic subjects. In addition to acetone, cross sensitivity of the sensor device for methanol and 2-propanol and humidity effect were also investigated.

D. Determination of Acetone Vapor Concentrations

The concentrations of these analytes were generated by flowing dry air through a bubbler (Fig. 10) contains traces concentrations of liquids of these analytes.

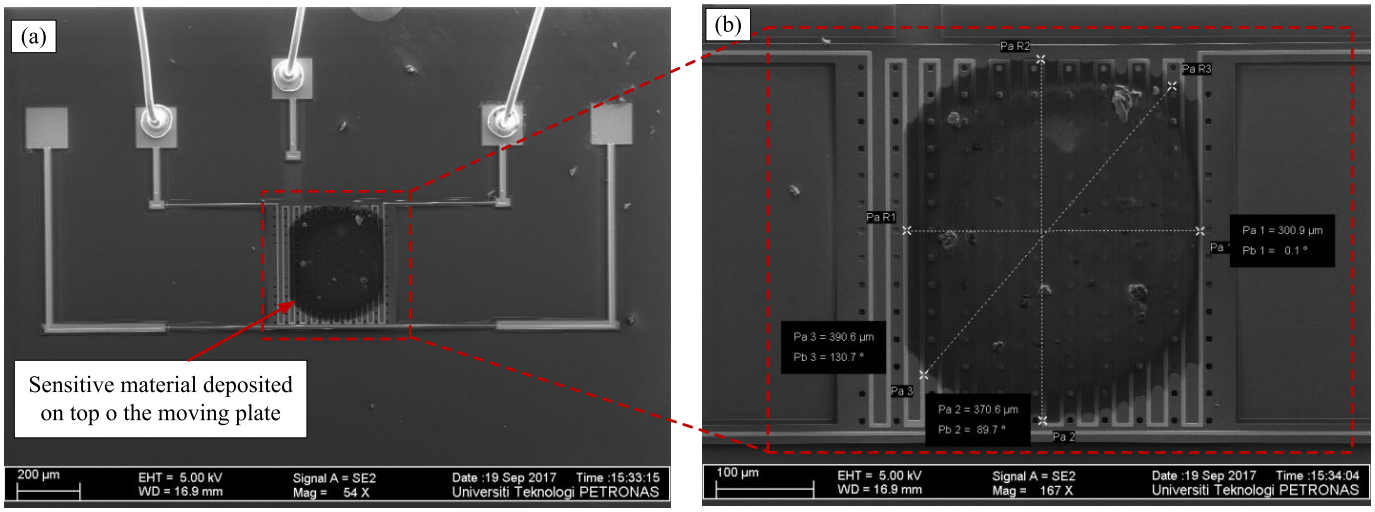

Fig. 6. FESEM image of the deposited device: (a) full device and (b) zoom in picture of the deposited moving plate.

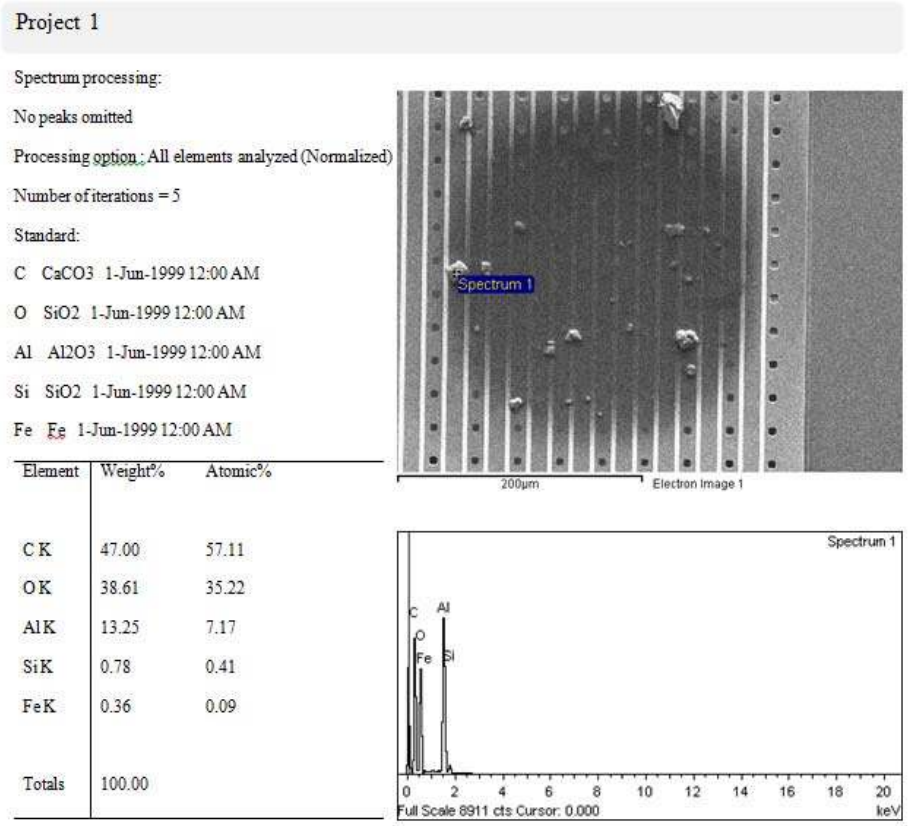

Fig. 7. FESEM of the deposited device and X-ray spectroscopy of the layer.

The air flow system shown in Fig. 10 has three paths. The first path is used to clean the test chamber prior to passing the analytes vapors into the chamber. In this path the dry air (purging air) is flown through valve 1, valve 2, valve 4, flow meter 1 and valve 7 to the chamber while all other valves and flow meters of the system are closed. Then another path (either the path of bubbler 1 or bubbler 2) is opened before the purging air is ceased of the chamber. The second path is used to control the humidity inside the test chamber, in which the dry air (carrier air) is flown through valve 1, valve 2, valve 5 to bubbler 2 to saturate with deionized (DI) water, then through flow meter 2 and valve 8 to the chamber while all other valves and flow meters are closed. The last path (the third path) the dry air (carrier air) is passed through valve 1, valve 3 to saturate with the analyte (acetone, methanol or 2-propanol) in bubbler 1, then the saturated air flows through flow meter 3, valve 6 and valve 8 to the test chamber.

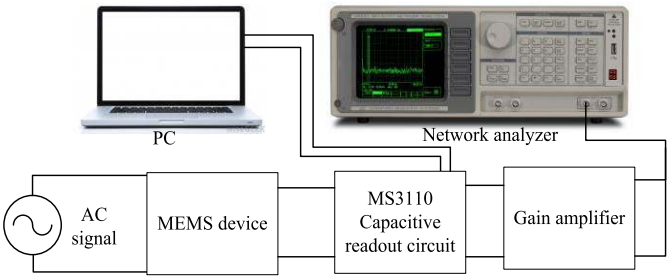

Fig. 8. Block diagram of the dynamic characterization setup.

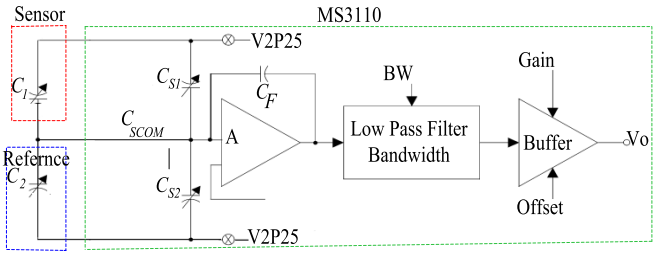

Fig. 9. Schematic diagram of the MS3110 capacitive readout circuit.

The required concentrations of acetone, methanol and 2-propanol were generated from 99.5% liquid solutions of these analytes purchased from Merck, Malaysia. Small concentrations of these analytes inside the bubbler were achieved by using (18).

$$C_1 V_1 = C_2 V_2 \tag{18}$$

where C_1 is the initial concentration of the analyte liquid (99.5%), V_1 is the amount of the liquid required to prepare the desired concentration C_2 in the bubbler, and V_2 is the final volume of the diluted concentration in the bubbler, which comprises the volume of both the diluted analyte and the dilute (DI water) compounds. The carrier air could be assumed to be fully saturated with the analyte liquid inside the bubbler [52]. Thus the final concentration of the analyte inside the test chamber will be the concentration of that analyte in the bubbler. The actual measurement setup for the dynamic characterization is shown in Figure 11.

IV. Results and Discussion

A. Modeling Results of the Device

The parameters that govern and resulted from the motion of the device were found by applying the formulas from (1) to (13), and the results are given in Table V.

TABLE V
Modeled Parameters of the Device

Parameter	Symbol	Unit	Value
Total mass of the device	m	kg	8.95×10^{-10}
Stiffness constant	k	N/m	2.7182
Total damping	b	Nm	4.0×10^{-5}
Undamped Resonance frequency	f	kHz	8.774
Mass sensitivity	S_m	mHz/pg	2.644
Quality factor	Q	-	1.04
Vapor concentration sensitivity	S_g	mHz/ppm	42.832
Detection limit	C_m	ppm	0.023
Bandwidth	BW	kHz	7.13
Static sensed capacitance	C_{s0}	fF	317
Resistance of microheater	R	Ω	131.23
Resistance of Temperature sensor	R	Ω	15.7863

B. Simulation Results of the Device

Simulation results were found by using Designer module of 2008 CoventorWare software and solving the design parameters using the Solver module of the Coventor. Fig. 12 shows the 3D model of the device.

The 3D model was meshed, and the solver module was used with suitable boundary conditions to obtain the resonance frequency of the first mode (out of plane vibration in the z-direction). Fig. 13 shows the FEA simulation of the modal displacement, showing the first mode resonance frequency at 8.718 kHz. As expected the vibration of the top moving plate is out of plane in the z-direction. This resonance frequency is close to the modeled resonance frequency (8.774 kHz), with a percentage difference of $\sim 0.64\%$.

FEA simulation was also performed by applying electric potential across the microheater terminals to determine the temperature distribution profile over the plate area. Maximum potential difference of 5 V was applied and Fig 14 shows the electric potential profile that decreases from the maximum value of 5 V to 0 V.

The corresponding temperature distribution on the surface of the moving plate was found and presented in Fig 15. It indicates a uniform temperature distribution over the plate area, with a maximum temperature of 850 K (577 °C) at the center of the plate, and a gradient between the center and the edge of the plate $\sim$0.006 °C/μm.

C. Dynamic Characterization Results

The sensor device was dynamically characterized using the setup shown in Fig. 8. An external reference ceramic capacitor C_2(1 pF) was connected in parallel with C_{s2}(0.798 pF) while C_1(0.317 pF) of the sensor device was connected in parallel with C_{s1}(2.052 pF) to form differential capacitance measurement. The device was driven using sinusoidal signal of 500 mVrms and the frequency of the driving signal was varied from 2 − 6 kHz, within the range of bandwidth of the readout circuit (0.5 − 8kHz). The output voltage of the readout circuit was amplified by factor of 10 using an external amplifier.

The output voltage of the sensor device was found to decrease by increasing the frequency of the driving signal. The maximum output voltage for the dry air was observed to be 11.78 V at 3 kHz driving frequency (Fig. 14). However, the signal stability was noticed to be better at higher driving frequencies compared to lower frequencies. Hence for the

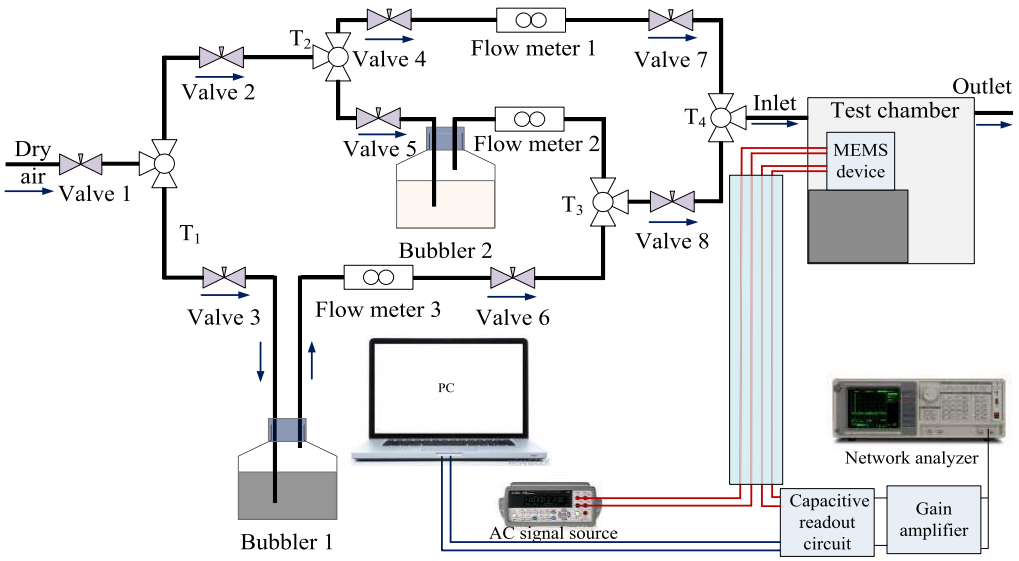

Fig. 10. Schematic of air flow system.

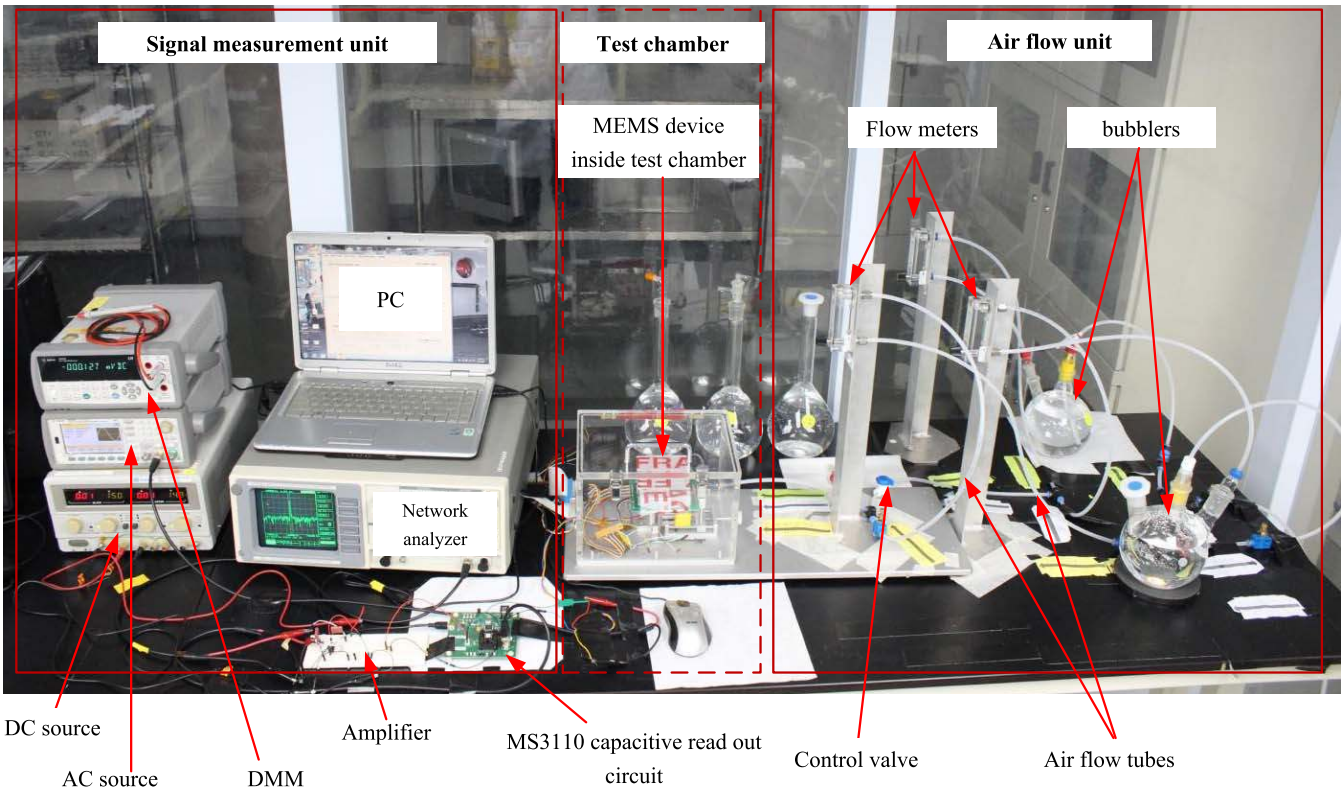

Fig. 11. The actual measurement setup.

acetone vapor testing 4 kHz driving frequency was used with the 500 mV actuation voltage. The output voltage at this frequency was found to be 11.30 V in the dry air.

D. Humidity Effect on the Output Signal of the Sensor Device

The effect of the humidity was investigated by passing the dry air through bubbler 2 (Fig. 10) having only the deionized water (DI) water. The response of the sensor device for full relative humidity of ~ 89.7% compared to its response in the dry air. As can be seen in Fig. 14, the sensor device was found to have response also to the humidified air, where the output voltage at 4 kHz driving frequency for the humidified air was found to be 11.41 V. This value gives a change of 110 mV from the dry air reading. Since the human breath is fully humidified, with ~ 90% relative humidity [53], [54], to accurately detect acetone in the exhaled breath the humidity effect on the sensor output is needed to be measured and cancelled.

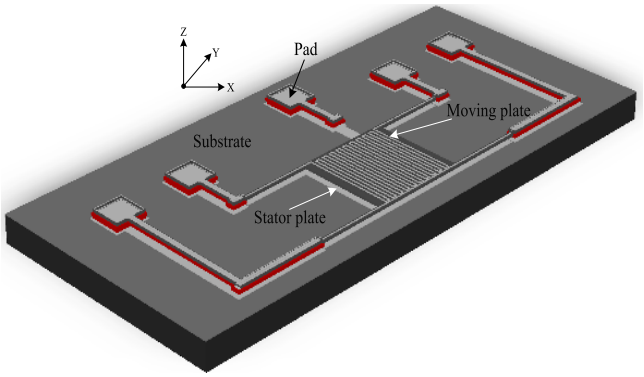

Fig. 12. The 3D model of the device.

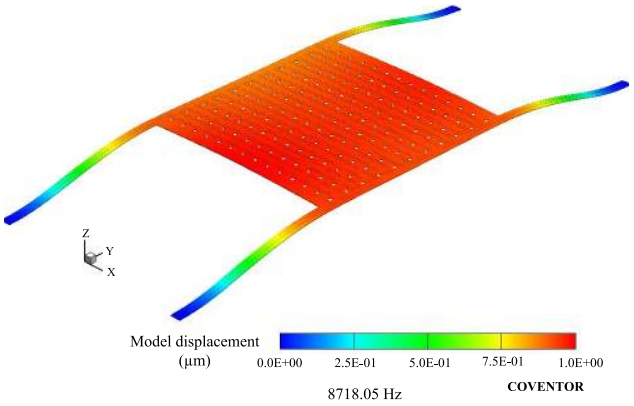

Fig. 13. FEA simulation results of modal displacement showing the resonance frequency at 8.718 kHz.

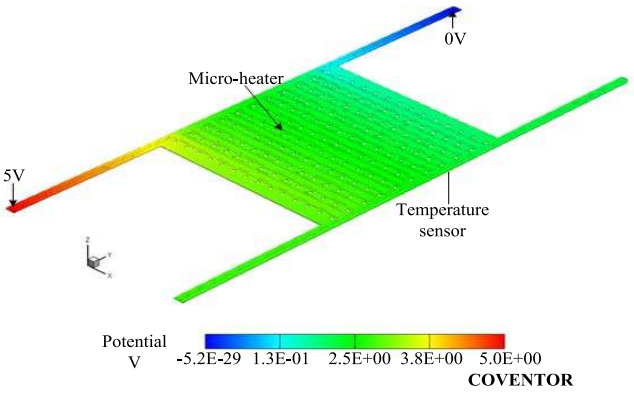

Fig. 14. A typical FEA simulation of the potential distribution along the micro-heater element.

TABLE VI
ACETONE VAPOR CONCENTRATIONS

V_1 (μL)	C_1 (%)	V_1 (L)	C_2 (ppm)
0.05	99.5	0.9	0.05
0.09	99.5	0.9	0.1
0.45	99.5	0.9	0.5
0.90	99.5	0.9	1
1.81	99.5	0.9	2
2.71	99.5	0.9	3
3.62	99.5	0.9	4
4.52	99.5	0.9	5

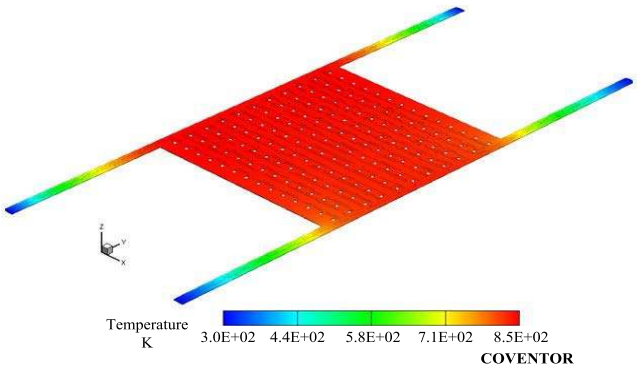

Fig. 15. Uniform temperature distribution on the surface of the moving plate.

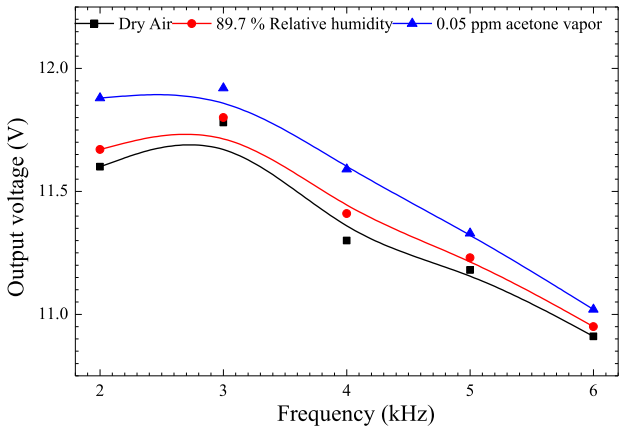

Fig. 16. Sensor response in dry air, humid air and 0.05 ppm acetone vapor.

E. Testing the Sensor Device for Acetone Vapors in Air

The device was tested for acetone vapor concentrations in the range of 0.05− 5 ppm. The acetone vapor concentrations were prepared by injecting tiny drops using Hamilton micro syringe needle or insulin injection syringe into 1 liter volumetric flask bubbler (bubbler 1). The right acetone concentrations inside the bubbler were determined by following the formula given in (12). TABLE VI shows the amounts of acetone liquid and DI water required to prepare the desired concentrations.

Fig. 14 shows the output voltage of the device in the dry air, humidified air and 0.05 ppm acetone vapor concentration. The output voltage of the sensor device for 0.05 ppm acetone vapor concentration has higher response compared to the output of the relative humidity; where at 4 kHz driving frequency the response for 0.05 ppm acetone vapor was found to be 11.59 V. This value gives changes of 180 mV and 290 mV, respectively from the readings of the sensor device in the humid and dry airs.

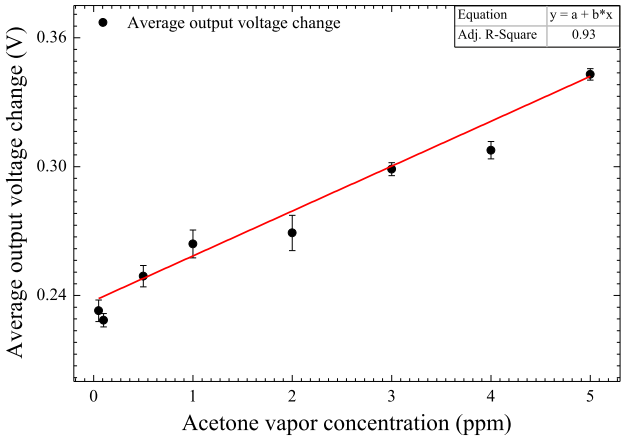

Fig. 17. Average output voltage change of the sensor device vs acetone vapor concentration in air.

The response of the sensor device for different concentrations (0.05 − 5 ppm) of acetone vapor as shown in TABLE VI was studied, and the output voltage of each at 4 kHz and 500 mV actuation voltage was recorded. The effect of the humidity was cancelled by subtracting the change due to the humidity from the change due to the acetone vapor. The measurement was repeated three times and the average output voltage change for the three runs at different acetone vapor concentrations is shown in Fig. 17. Fig. 17 depicts that the average output voltage is linearly correlated to the acetone vapor concentration in air with a correlation factor of 0.93. It increases from 0.233 V at the acetone vapor concentration of 0.05 ppm to 0.343 V when the acetone vapor concentration is 5 ppm. This graph gives a sensitivity of 0.021 V/ppm. By having this good relation and correlation the device is believed to be capable to use for acetone vapor sensing in the exhaled breath for diabetes screening. As mentioned in the literature review part, diabetic subjects have exhaled acetone vapor of more than 1.8 ppm.

F. Noise Analysis and Experimental Limit of Detection

The output of the device was measured using the universal MS3110 capacitive readout circuit. This readout circuit has a resolution of 4 aF/$\sqrt{\text{Hz}}$ [55]. To analyze the noise of the system the noise floor was measured prior to device excitation, and it was found to be 32.54 mV as shown in Fig 18.

This noise floor is amplified by the external amplifier of a factor of 10; as such the real noise floor would be 3.254 mV. This small output fluctuation is equivalent to capacitance change of xx, that found using (19).

$$\Delta C = C_F \times \frac{\Delta(V_{out} - V_{ref})}{V_{ref} \times 1.14 \times 2} \tag{19}$$

The noise floor is not only due to system but is also a result of stray capacitance C_P of the connection leads that added to the system capacitance. Without stray capacitance the capacitance change will be given by (20), while with the stray capacitance

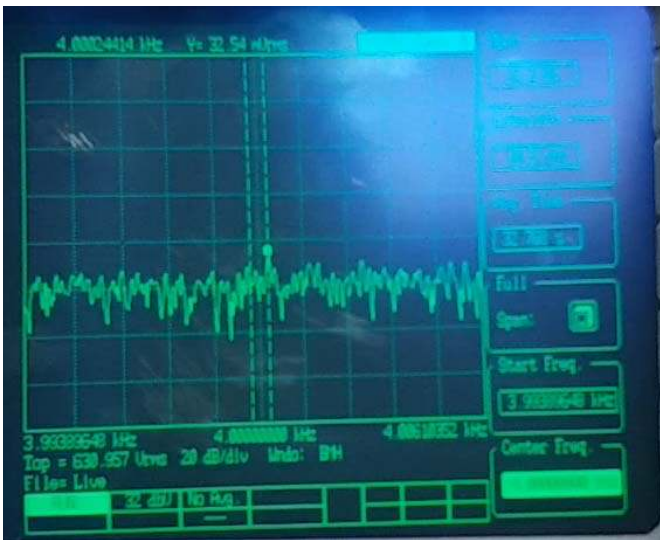

Fig. 18. The noise floor of the system.

the change is given by (21).

$$\Delta C = C_{T2} - C_{T1} \tag{20}$$

$$\Delta C = C_{T2} - C_{T1} \pm C_P \tag{21}$$

By calculating the values of C_{T2} and C_{T1} and measuring the output of the noise floor before and after connecting the device, the parasitic capacitance was found to be 0.758 pF. When the device is actuated the change in the capacitance is given by (22).

$$\Delta C = C_{T2} - (C_{T1} + \Delta C_{s1}) \pm C_P \tag{22}$$

The output voltage of the actuated device was measured and the noise floor was subtracted before the value is used to find the equivalent capacitance change. By eliminating the parasitic capacitance the capacitance change was found to be 0.0369 pF.

The minimum detectable voltage change is determined by the resolution of the SR770 Network analyzer used to measure the response of the device. This resolution is given to be 0.1 mVpk for the output voltage less than 100 mVpk and 1 mV for the output voltage greater than 100 mVpk [56]. The corresponding minimum detectable concentration is found from the sensitivity of the device and the resolution of the network analyzer. As mentioned before the sensitivity of the device was found to be 21 mV/ppm. This sensitivity relates the voltage change with the acetone vapor concentration, and can be written as in (23).

$$Sensitivity = \frac{\Delta V}{\Delta C_g} = \frac{21\text{mV}}{\text{ppm}} \tag{23}$$

Since response of the device is linear, from (23) the minimum detectable concentration corresponding to minimum detectable voltage change (resolution) is found to be 0.005 ppm.

G. Recovery and Response Time of the Sensor Device

To study the recovery and response time of the sensor device, the actuation voltage and the driving frequency were maintained fixed to 500 mVrms and 4 kHz, respectively.

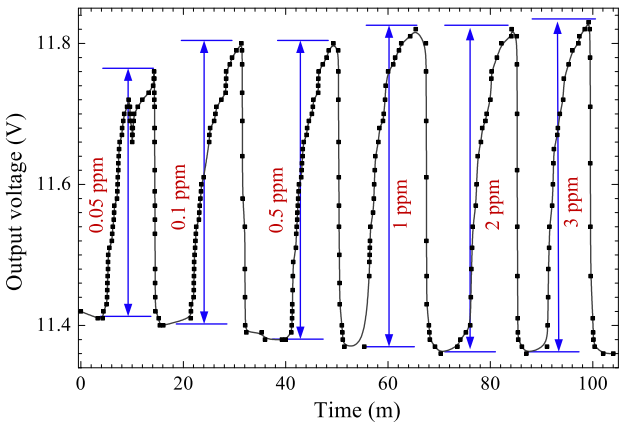

Fig. 19. Response of the sensor for different acetone vapor concentrations.

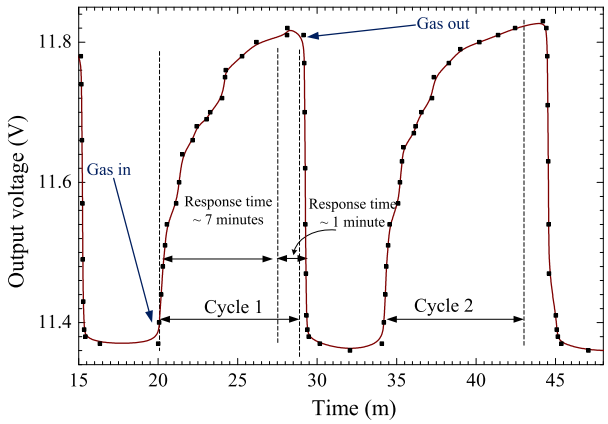

Fig. 20. Response and recovery times for two cycles of 1 ppm acetone vapor.

Response time is defined as the time taken by the device to attain 90 % of the final value of the output signal, while the recovery time is defined as the time taken by the device to regain 10 % of the base value. The response time was found by supplying the carrier air through valve 1, valve 3, flow meter 3, valve 6 and valve 8 into bubbler 1 of a defined acetone vapor concentration, and the output voltage of the network analyzer was monitored until there was no significant change observed. For the recovery time the purging air was used to clean the chamber using valve 1, valve 2, valve 4, flow meter 1 and valve 7. Fig. 19 shows the plot of the output voltage versus the response and recovery time of the device for different acetone vapor concentrations.

It was observed that there was no significant difference between recovery and response times for the different acetone concentrations. Fig. 20 shows two cycles of recovery and response times for 1 ppm acetone vapor concentration.

As shown by Fig. 20, the response time was found to be ∼7 minute, while the recovery time was found to be ∼1 minute, and the measurement shows good repeatability.

H. Cross-Sensitivity and Selectivity Test of the Sensor Device

Cross- sensitivity test of the sensor device was performed by examining the sensor response to 2-propanol and methanol, by preparing concentrations of 5 ppm for each one of the analytes using the same formula described in (12). Dry air was purged into the test chamber to clean it from any molecules inside the chamber and reading of the device in dry air was taken as the baseline. Then the carrier air was passed through bubbler 2 filled with 900 ml of DI water to bring the humidity inside the test chamber to ∼90 %RH, and the response of the sensor to humidity was recorded. Then the second path of the bubbler (bubbler 1) with analytes was used to pass the carrier air through to saturate and carry the analyte into the test chamber. The output voltage was recorded after 5 minutes of the continuous supply of the 5 ppm concentration of the analyte. After measuring the response of the sensor for each analyte the effect of the humidity was cancelled by subtracting the analyte reading from both the humidity and dry air readings. Fig 21 gives the output voltage change for each analyte measured from the baseline voltage after eliminating the effect of the relative humidity.

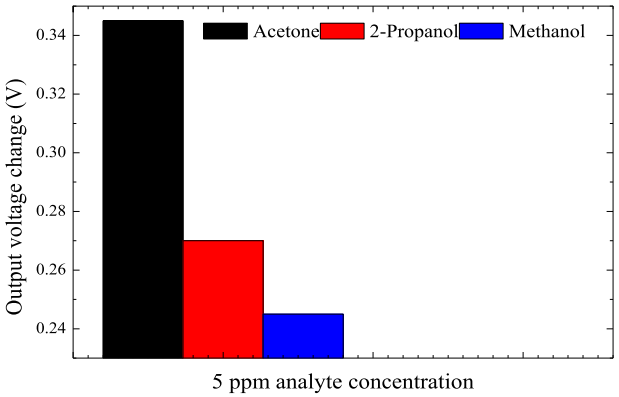

Fig. 21. Sensor device response for different analytes.

The change in the output voltage for 5 ppm acetone vapor concentration was found to be 0.345 V, while for 2-propanol and methanol the output voltage change was found to be 0.27 V and 0.245 V, respectively. It is therefore, the output voltage change for the 5 ppm concentration of acetone vapor is ∼ 24% and 33% higher than the output voltage change for 5ppm concentration of the 2-propanol and 5 ppm concentration of methanol, respectively.

I. Sensor Device Compared to Published Acetone Vapor Sensors

Table VII compares the proposed sensor device with some of the published papers in term of sensing layer, detection limit and working temperature.

This proposed sensor device for acetone vapor sensing for the possible use for non-invasive screening of diabetes is functionalized with blend of chitosan/PEG polymers as sensing layer. The output signal change of the sensor device relies on absorption/adsorption of the acetone molecules on the surface of the sensing layer. As such the mass of the moving plate changes which will affect the output of the sensor. This mass loading does not require elevating temperatures as required by majority of metal oxide semiconductor sensors used in literature for acetone vapor sensing. As can be seen in TABLE VII, most of the published sensors work at high

TABLE VII
COMPARISON OF THE PROPOSED SENSOR DEVICE TO SOME PUBLISHED PAPERS

Sensing layer	Detection limit (ppm)	Working temperature (°C)	Ref
Zinc oxide (ZnO)	1000	325	[57]
Ferroeletric tungustin trioxide	0.20	500	[58]
Indium nitride (InN) catalyzed with Pt	0.4	200	[30]
SnO_2 functionalized with Pt and Au	0.10	350	[59]
Indium oxide nanowires	25	400	[60]
Tin oxide (SnO_2) catalysed with Pt	0.12	300	[61]
Nano structured anatase of titanium oxide	1	500	[62]
Pt-Functionalized tungustin oxide	0.12	300	[63]
Sr-doped Lanthanum orthoferrite	500	275	[64]
WO_3 functionalized by Rh_2O_3	0.10	350	[65]
ε -WO_3 doped with Cr	0.20	400	[66]
Ni-doped Zinc oxide (ZnO) nanorods	100	RT	[67]
Hematite (α-Fe_2O_3)	1	265	[68]
Poly(butylmethacrylate) (PBMA)	5.5	RT	[69]
([bmim][BF4])	5	RT	[70]
Chitosan	0.1	RT	[71]
Chitosan/PEG	0.05	RT	This work

temperatures because they are based on metal oxide semiconducting materials which depend on the resistance change of the sensing layer films upon exposure to acetone vapor. In addition, some of these sensors do not show enough sensitivity to be used for non-invasive screening of diabetes. There are some sensors that work at room temperatures. However, these sensors' limit of detection is above 1.8 ppm (this concentration is considered as the threshold of the exhaled acetone in the human breath for the diabetic subjects). In our current work, we have proposed to use a blend of chitosan/PEG polymers as a sensing layer, and the sensing mechanism is based on frequency /or amplitude change due to the change of mass of the sensors device upon adsorption/desorption of acetone vapor by the deposited layer.

V. LIMITATIONS OF THE STUDY AND FUTURE RECOMMENDATIONS

Acetone vapor concentration was generated using a bubbler with an uncontrolled temperature, where the bubbler and the vapor temperature was assumed to be constant and equal to room temperature. Thus it is recommended to use a controlled temperature bath bubbler to control the temperature which arises due to heat losses as a result of liquid evaporation [72].

Fig. 19 shows that there is an apparent baseline drift in the output voltage of the device. It could be due to frequency drift, which is known to be common in silicon MEMS resonators. To compensate the frequency drift the resonant frequency of the device could be made dependent on the bias voltage, and this voltage is adjusted when the drift is detected [73]. Another way to minimize frequency drift is to operate the resonator in a temperature controlled environment; in which an optimum temperature control with quick settling time is provided [74].

The testing measurement was conducted for increasing concentrations from low to high, therefore it is recommended to test the sensor also for the decreasing concentrations from high to low. In addition, to improve sensitivity and accuracy of the system, the device is recommended to run inside a vacuum and at its resonance frequency.

VI. CONCLUSION

This paper presented MEMS sensor device fabricated using PolyMUMPs technology, and proposed for use to detect acetone vapor in the exhaled breath for possible non-invasive screening of diabetes. The sensor is actuated using electrothermal means by having a microheater, while the output signal is measured using MS3110 capacitive readout circuit. The device was experimentally tested by depositing it with a blend of chitosan/PEG polymers. Linear output voltage change was found for 0.05 ppm − 5 ppm acetone vapor concentration, with a correlation factor of 0.93 and sensitivity of 21 mV/ppm. The response time of the sensor was found to be ∼7 minute, while the recovery time was found to be ∼1 minute. The cross-sensitivity test for 5 ppm of 2-propanol and methanol gives ∼ 24% and 33% lower response respectively compared to the response of the sensor for 5ppm acetone vapor. Thus, this device could be further developed and used for acetone vapor sensing in exhaled breath for possible non-invasive screening of diabetes.

REFERENCES

[1] C.-F. So, K.-S. Choi, T. K. Wong, and J. W. Chung, "Recent advances in noninvasive glucose monitoring," *Med. Devices, Evidence Res.*, vol. 5, pp. 45–52, Jun. 2012.
[2] C. Turner, C. Walton, S. Hoashi, and M. Evans, "Breath acetone concentration decreases with blood glucose concentration in type I diabetes mellitus patients during hypoglycaemic clamps," *J. Breath Res.*, vol. 3, no. 4, p. 046004, 2009.
[3] A. E. Heath, "Comparison of screening methods for prediabetes and type 2 diabetes mellitus by race/ethnicity and gender," M.S. thesis, Inst. Public Health, Georgia State Univ., Atlanta, GA, USA, 2012.
[4] O. E. Owen *et al.*, "Acetone metabolism during diabetic ketoacidosis," *Diabetes*, vol. 31, no. 3, pp. 242–248, 1982.
[5] S. F. Clarke and J. R. Foster, "A history of blood glucose meters and their role in self-monitoring of diabetes mellitus," *Brit. J. Biomed. Sci.*, vol. 69, no. 2, pp. 83–93, 2012.
[6] P. Patel and A. Macerollo, "Diabetes mellitus: Diagnosis and screening," *Amer. Family Physician*, vol. 81, no. 7, pp. 863–870, 2010.
[7] US Department of Health and Human Services, *Diagnosis of Diabetes*, New York, NY, USA: National Diabetes Information Clearinghouse, 2008

[8] W. H. Herman and S. S. Fajans, "Hemoglobin A1c for the diagnosis of diabetes: Practical considerations," *Polskie Archiwum Medycyny Wewnetrznej*, vol. 120, nos. 1–2, pp. 37–41, 2010.

[9] T. Nakagami *et al.*, "Combined use of fasting plasma glucose and glycated hemoglobin A1c in a stepwise fashion to detect undiagnosed diabetes mellitus," *J. Exp. Med.*, vol. 213, pp. 25–32, 2007.

[10] *Guideline on Clinical Investigation of Medicinal Products in the Treatment or Prevention of Diabetes Mellitus*, European Medicines Agency, London, U.K., 2012.

[11] American Diabetes Association, "Diagnosis and classification of diabetes mellitus," *Diabetes Care*, vol. 31, no. 1, pp. S62–S69, 2008.

[12] *In the Clinic: Type 2 Diabetes*, Amer. College Physicians (ACP), Philadelphia, PA, USA, 2010.

[13] M. Gupta and H. Aggarwal, "Design and implementation of PSoC based cap sense for medical touch system saliva vs blood glucose meter," *Int. J. Adv. Res. Comput. Sci. Softw. Eng.*, vol. 3, no. 5, pp. 1172–1186, 2013.

[14] S. K. Vashist, "Continuous glucose monitoring systems: A review," *Diagnostics*, vol. 3, no. 4, pp. 385–412, Oct. 2013.

[15] J. Kaur, J. Kumar, H. K. Sardana, R. Bhatnagar, and N. S. Mehla, "Non invasive blood glucose measurement using optical method: Feasibility study and design issues," Presented at the ICOP-Int. Conf. Opt. Photon., Chandigarh, India, 2009, pp. 1–4.

[16] H. Reinauer, P. D. Home, A. S. Kanagasabapathy, and C.-C. Heuck, "Laboratory diagnosis and monitoring of diabetes mellitus," World Health Org., Geneva, Switzerland, Tech. Rep., 2002.

[17] B. Zeng, W. Wang, N. Wang, F. Li, F. Zhai, and L. Hu, "Noninvasive blood glucose monitoring system based on distributed multi-sensors information fusion of multi-wavelength NIR," *Engineering*, vol. 5, no. 10B, pp. 553–560, 2013.

[18] D. Guo, D. Zhang, N. Li, L. Zhang, and J. Yang, "A novel breath analysis system based on electronic olfaction," *IEEE Trans. Biomed. Eng.*, vol. 57, no. 11, pp. 2753–2763, Nov. 2010.

[19] W. Cao and Y. Duan, "Breath analysis: Potential for clinical diagnosis and exposure assessment," *Clin. Chem.*, vol. 52, no. 5, pp. 800–811, 2006.

[20] A. J. A. McGuinness and E. Sapey, "Oxidative stress in COPD: Sources, markers, and potential mechanisms," *J. Clin. Med.*, vol. 6, no. 2, p. 21, 2017.

[21] N. K. Kozij, J. T. Granton, P. E. Silkoff, J. Thenganatt, S. Chakravorty, and S. R. Johnson, "Exhaled nitric oxide in systemic sclerosis lung disease," *Can. Respiratory J.*, vol. 2017, Feb. 2017, Art. no. 6736239.

[22] K. Iwayama *et al.*, "Long-term treatment of clarithromycin at a low concentration improves hydrogen peroxide-induced oxidant/antioxidant imbalance in human small airway epithelial cells by increasing Nrf2 mRNA expression," *BMC Pharmacol. Toxicol.*, vol. 18, no. 1, p. 15, 2017.

[23] J. Obermeier *et al.*, "Exhaled volatile substances mirror clinical conditions in pediatric chronic kidney disease," *PLoS ONE*, vol. 12, no. 6, p. e0178745, 2017.

[24] C. Wang and A. B. Surampudi, "An acetone breath analyzer using cavity ringdown spectroscopy: An initial test with human subjects under various situations," *Meas. Sci. Technol.*, vol. 19, no. 10, p. 105604, 2008.

[25] V. Ruzsányi and M. P. Kalapos, "Breath acetone as a potential marker in clinical practice," *J. Breath Res.*, vol. 11, no. 2, p. 024002, 2017.

[26] C. Deng, J. Zhang, X. Yu, W. Zhang, and X. Zhang, "Determination of acetone in human breath by gas chromatography–mass spectrometry and solid-phase microextraction with on-fiber derivatization," *J. Chromatography B*, vol. 810, no. 2, pp. 269–275, 2004.

[27] M. Righettoni, A. Tricoli, and S. E. Pratsinis, "Si: WO_3 sensors for highly selective detection of acetone for easy diagnosis of diabetes by breath analysis," *Anal. Chem.*, vol. 82, no. 9, pp. 3581–3587, 2010.

[28] P. R. Galassetti *et al.*, "Breath ethanol and acetone as indicators of serum glucose levels: An initial report," *Diabetes Technol. Therapeutics*, vol. 7, no. 1, pp. 115–123, 2005.

[29] K. Musa-Veloso, S. S. Likhodii, and S. C. Cunnane, "Breath acetone is a reliable indicator of ketosis in adults consuming ketogenic meals," *Amer. J. Clin. Nutrition*, vol. 76, no. 1, pp. 65–70, 2002.

[30] K.-W. Kao, M.-C. Hsu, Y.-H. Chang, S. Gwo, and J. A. Yeh, "A sub-ppm acetone gas sensor for diabetes detection using 10 nm thick ultrathin InN FETs," *Sensors*, vol. 12, no. 6, pp. 7157–7168, 2012.

[31] I. F. Rivera, "RF MEMS resonators for mass sensing applications," Ph.D. dissertation, Dept. Elect. Eng., Univ. South Florida, Tampa, FL, USA, 2015.

[32] A. D'Amico, C. Di Natale, L. Mosiello, and G. Zappa, "Sensors and microsystems," in *Proc. AISEM*, 2011, pp. 157–158.

[33] L. Kosuru, A. Bouchaala, N. Jaber, and M. I. Younis, "Humidity detection using metal organic framework coated on QCM," *J. Sensors*, vol. 2016, Jun. 2016, Art. no. 4902790.

[34] Z. Ying, Y. Jiang, H. Qin, L. Zheng, and X. Du, "A study on QCM sensor for identification of acetone vapor," *Int. J. Comput. Math. Elect. Electron. Eng.*, vol. 29, no. 2, pp. 477–483, 2010.

[35] A. A. S. Rabih *et al.*, "MetalMUMPs resonator for acetone vapor sensing," in *Proc. IEEE Regional Symp. Micro Nanoelectron. (RSM)*, Batu Ferringhi, Malaysia, Aug. 2017, pp. 5–9.

[36] C. Liu, *Foundations of MEMS*. London, U.K.: Pearson Education, 2006.

[37] W. Wai-Chi, A. A. Azid, and B. Y. Majlis, "Formulation of stiffness constant and effective mass for a folded beam," *Arch. Mech*, vol. 62, no. 5, pp. 405–418, 2010.

[38] H. Sumali, "Squeeze-film damping in the free molecular regime: Model validation and measurement on a MEMS," *J. Micromech. Microeng.*, vol. 17, no. 11, pp. 2231–2240, Nov. 2007.

[39] M. I. Younis, *MEMS Linear and Nonlinear Statics and Dynamics*. Berlin, Germany: Springer, 2011.

[40] M. J. Novack, "Design and fabrication of a thin film micromachined accelerometer," M.S. thesis, Dept. Mech. Eng., Massachusetts Inst. Technol., Cambridge, MA, USA, 1992.

[41] J. O. Dennis, A. Y. Ahmed, M. H. M. Khir, and A. A. S. Rabih, "Modelling and simulation of the effect of air damping on the frequency and quality factor of a CMOS-MEMS resonator," *Appl. Math. Inf. Sci.*, vol. 9, no. 2, pp. 729–737, 2015.

[42] A. A. S. Rabih, J. O. Dennis, M. H. M. Khir, and M. A. Abdullah, "Design, modeling and simulation of CMOS-MEMS resonator for biomedical application," in *Proc. 5th Int. Conf. Intell. Adv. Syst. (ICIAS)*, Jun. 2014, pp. 1–6.

[43] M. A. Anwar, M. Packirisamy, and A. K. W. Ahmed, "Disc type thermal actuator with straight beams for angular motion," *Appl. Thermal Eng.*, vol. 51, nos. 1–2, pp. 988–999, 2013.

[44] W. M. Zhang, K. M. Hu, Z. K. Peng, and G. Meng, "Tunable micro- and nanomechanical resonators," *Sensors*, vol. 15, no. 10, pp. 26478–26566, Oct. 2015.

[45] G. Demirhan, "Resonance-based MEMS temperature sensors for temperature compensation of MEMS capacitive accelerometer," M.S. thesis, Dept. Elect. Electron. Eng., Middle East Tech. Univ., Ankara, Turkey, 2016.

[46] Y. Chang *et al.*, "Detection of volatile organic compounds by self-assembled monolayer coated sensor array with concentration-independent fingerprints," *Sci. Rep.*, vol. 6, Apr. 2016, Art. no. 23970.

[47] E. A. El-Hefian, M. M. Nasef, and A. H. Yahaya, "Chitosan-based polymer blends: Current status and applications," *J. Chem. Soc. Pakistan*, vol. 36, no. 1, pp. 11–27, 2014.

[48] S. K. Shukla, A. K. Mishra, O. A. Arotiba, and B. B. Mamba, "Chitosan-based nanomaterials: A state-of-the-art review," *Int. J. Biol. Macromolecules*, vol. 59, pp. 46–58, Aug. 2013.

[49] M. Zhang, X. H. Li, Y. D. Gong, N. M. Zhao, and X. F. Zhang, "Properties and biocompatibility of chitosan films modified by blending with PEG," *Biomaterials*, vol. 23, no. 13, pp. 2641–2648, 2002.

[50] Q. Zhang, "Investigating polymer conformation in poly (ethylene oxide) (PEO) based systems for pharmaceutical applications," M.S. thesis, Dept. Appl. Phys., Chalmers Univ. Technol., Göteborg, Sweden, 2011.

[51] J.-K. F. Suh and H. W. T. Matthew, "Application of chitosan-based polysaccharide biomaterials in cartilage tissue engineering: A review," *Biomaterials*, vol. 21, no. 24, pp. 2589–2598, 2000.

[52] A. W. Weimer, *Carbide, Nitride and Boride Materials Synthesis and Processing*. London, U.K.: Chapman & Hall, 1997.

[53] T. A. Vincent, B. Urasinska-Wojcik, and J. W. Gardner, "Development of a low-cost NDIR system for ppm detection of carbon dioxide in exhaled breath analysis," *Procedia Eng.*, vol. 120, pp. 388–391, Jan. 2015.

[54] T. L. Mathew, P. Pownraj, S. Abdulla, and B. Pullithadathil, "Technologies for clinical diagnosis using expired human breath analysis," *Diagnostics*, vol. 5, no. 1, pp. 27–60, 2015.

[55] K. Simsek, "Developing a capacitance readout circuitry for a directional MEMS sound sensor and sound source localization in a sensor network environment," M.S. thesis, Dept. Elect. Eng., Naval Postgraduate School, Monterey, CA, USA, 2009.

[56] *User's Manual: Model SR770 FFT Network Analyzer*, SRS Inc., Sunnyvale, CA, USA, 2006.

[57] P. P. Sahay, "Zinc oxide thin film gas sensor for detection of acetone," *J. Mater. Sci.*, vol. 40, no. 16, pp. 4383–4385, 2005.

[58] L. Wang, K. Kalyanasundaram, M. Stanacevic, and P. Gouma, "Nanosensor device for breath acetone detection," *Sensor Lett.*, vol. 8, no. 5, pp. 709–712, 2010.
[59] J.-S. Jang *et al.*, "Thin-walled SnO_2 nanotubes functionalized with Pt and Au catalysts *via* the protein templating route and their selective detection of acetone and hydrogen sulfide molecules," *Nanoscale*, vol. 7, no. 39, pp. 16417–16426, 2015.
[60] A. Vomiero, S. Bianchi, E. Comini, G. Faglia, M. Ferroni, and G. Sberveglieri, "Controlled growth and sensing properties of In_2O_3 nanowires," *Cryst. Growth Des.*, vol. 7, no. 12, pp. 2500–2504, 2007.
[61] J. Shin *et al.*, "Thin-wall assembled SnO_2 fibers functionalized by catalytic Pt nanoparticles and their superior exhaled-breath-sensing properties for the diagnosis of diabetes," *Adv. Funct. Mater.*, vol. 23, no. 19, pp. 2357–2367, 2013.
[62] A. Teleki, S. E. Pratsinis, K. Kalyanasundaram, and P. I. Gouma, "Sensing of organic vapors by flame-made TiO_2 nanoparticles," *Sens. Actuators B, Chem.*, vol. 119, no. 2, pp. 683–690, 2006.
[63] S.-J. Choi *et al.*, "Selective diagnosis of diabetes using Pt-functionalized WO_3 hemitube networks as a sensing layer of acetone in exhaled breath," *Anal. Chem.*, vol. 85, no. 3, pp. 1792–1796, 2013.
[64] P. A. Murade, V. S. Sangawar, G. N. Chaudhari, V. D. Kapse, and A. U. Bajpeyee, "Acetone gas-sensing performance of Sr-doped nanostructured $LaFeO_3$ semiconductor prepared by citrate sol–gel route," *Current Appl. Phys.*, vol. 11, no. 3, pp. 451–456, 2011.
[65] N.-H. Kim *et al.*, "Highly sensitive and selective acetone sensing performance of WO_3 nanofibers functionalized by Rh_2O_3 nanoparticles," *Sens. Actuators B, Chem.*, vol. 224, pp. 185–192, Mar. 2016.
[66] L. Wang, A. Teleki, S. E. Pratsinis, and P. I. Gouma, "Ferroelectric WO_3 nanoparticles for acetone selective detection," *Chem. Mater.*, vol. 20, no. 15, pp. 4794–4796, 2008.
[67] H. Ahn, Y. Wang, S. H. Jee, M. Park, Y. S. Yoon, and D.-J. Kim, "Enhanced UV activation of electrochemically doped Ni in ZnO nanorods for room temperature acetone sensing," *Chem. Phys. Lett.*, vol. 511, nos. 4–6, pp. 331–335, 2011.
[68] M.-Z. Yang, C.-L. Dai, and P.-J. Shih, "An acetone microsensor with a ring oscillator circuit fabricated using the commercial 0.18 μm CMOS Process," *Sensors*, vol. 14, no. 7, pp. 12735–12747, 2014.
[69] K. L. Dorsey, S. S. Bedair, and G. K. Fedder, "Gas chemical sensitivity of a CMOS MEMS cantilever functionalized via evaporation driven assembly," *J. Micromech. Microeng.*, vol. 24, no. 7, p. 075001, 2014.
[70] W. Tao, P. Lin, S. Liu, Q. Xie, S. Ke, and X. Zeng, "1-butyl-3-methylimidazolium tetrafluoroborate film as a highly selective sensing material for non-invasive detection of acetone using a quartz crystal microbalance," *Sensors*, vol. 17, no. 1, p. 194, 2017.
[71] T. I. Nasution, I. Nainggolan, S. D. Hutagalung, K. R. Ahmad, and Z. A. Ahmad, "The sensing mechanism and detection of low concentration acetone using chitosan-based sensors," *Sens. Actuators B, Chem.*, vol. 177, pp. 522–528, Feb. 2013.
[72] A. Love, S. Middleman, and A. K. Hochberg, "The dynamics of bubblers as vapor delivery systems," *J. Cryst. Growth*, vol. 129, nos. 1–2, pp. 119–133, 1993.
[73] A. Pomarico, A. Morea, P. Flora, G. Roselli, and E. Lasalandra, "Vertical MEMS resonators for real-time clock applications," *J. Sensors*, vol. 2010, Oct. 2010, Art. no. 362439.
[74] M. Rais-Zadeh, V. A. Thakar, Z. Wu, and A. Peczalski, "Temperature compensated silicon resonators for space applications," *Proc. SPIE*, vol. 8614, pp. 86140E-1–86140E-4, 2013.

Almur A. S. Rabih (M'09) was born in Sudan in 1983. He received the B.Sc. (Hons.) degree in electronic engineering (specialization in medical instrumentation) from the University of Gezira, Wad Medani, Sudan, in 2008, and the M.Sc. and Ph.D. degrees in electrical and electronic engineering from Universiti Teknologi PETRONAS, Perak, Malaysia, in 2012 and 2018, respectively. He then joined the University of Gezira as a Teaching Assistant. His area of focus is bio-MEMS, medical devices, and breath analysis.

J. O. Dennis (SM'16) was born in South Sudan in 1959. He received the B.Ed. (science) degree in mathematics and physics from the University of Juba, Juba, South Sudan, in 1982, and the Ph.D. degree in applied physics from the Universiti Teknologi Malaysia, Malaysia, in 2001. He joined the Electrical and Electronic Engineering Department, Universiti Teknologi PETRONAS, in 2003, as a Senior Lecturer. He is currently an Associate Professor with the Department of Fundamental and Applied Sciences, Universiti Teknologi PETRONAS. His current focus of research is in microelectromechanical systems design, simulation, and fabrication.

A. Y. Ahmed (M'08) was born in Sudan in 1980. He received the B.Sc. (Hons.) degree in electronic engineering from the University of Gezira, Wad Medani, Sudan, in 2006, and the M.Sc. and Ph.D. degrees in electrical and electronics engineering from Universiti Teknologi PETRONAS, Malaysia, in 2009 and 2015, respectively. He joined Universiti Teknologi PETRONAS in 2016, where he is currently a Lecturer with the Electrical and Electronic Engineering Department. The area of focus is microelectromechanical systems (MEMS) actuator/sensor design and microfabrication/sensor technology based on CMOS-MEMS technologies.

M. H. Md Khir (M'08) was born in Kedah, Malaysia, in 1968. He received the B.Eng. degree in electrical and electronic engineering from the Universiti Teknologi MARA, Selangor, Malaysia, in 1999, and the M.Sc. degree in computer. He joined Universiti Teknologi PETRONAS in 1999, where he is currently an Associate Professor with the Electrical and Electronic Engineering Department. His research interest is in micro/nano–electro-mechanical systems sensors and actuator development. Most sensors and actuators devices fabricated were based on CMOS and MUMPS technologies.

Mawahib G. A. Ahmed (M'16) was born in Sudan in 1975. She received the B.Sc. (Hons.) degree in electronics engineering (specialization in biomedical engineering) from the University of Gezira, Wad Medani, Sudan, in 2008, then she joined the Department of Electronics Engineering, University of Gezira, in 2004, as a Teaching Assistant. He received the M.Sc. and Ph.D. degrees in electrical and electronic engineering from Universiti Teknologi PETRONAS, Perak, Malaysia, in 2009 and 2017, respectively. She is currently an Assistant Professor with the Department of Electronic Engineering (Biomedical Engineering), University of Gezira. Her current focus of research is breath analysis using microelectromechanical systems and early detection of cancer using image processing.

Alamin Idris was born in Saudi Arabia in 1983. He received the B.E. degree in chemical engineering from Visveswaraia Technological University, Karnataka, India, in 2007, the M.Tech. degree in chemical engineering from the Siddaganga Institute of Technology, Tumkur, Karnataka, in 2011, and the Ph.D. degree from Universiti Teknologi PETRONAS in membrane science and technology. Besides his major research area, he is active and working in the area of organic coatings, polymer science, ionic liquids, polymer-inorganic nancomposites, and gas separation.

Muhammad Umer Mian received the B.S. degree in electronics from the COMSATS Institute of Information Technology, Islamabad, Pakistan, in 2009, the M.Sc. degree in electronic engineering from the Ghulam Ishaq Khan Institute GIKI, Topi, Pakistan, in 2011, and the Ph.D. degree in electrical and electronics engineering from Universiti Teknologi PETRONAS, Malaysia, in 2018. His area of interest is MEMS inertial sensors and BioMEMS.